Engineering Fracture Mechanics 292 (2023) 109632

Contents lists available at ScienceDirect

Engineering Fracture Mechanics

journal homepage: www.elsevier.com/locate/engfracmech

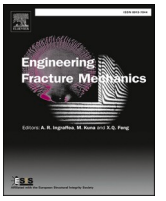

An enhanced lattice beam element model for the numerical simulation of rate-dependent self-healing in cementitious materials

Sina Sayadi [a,*], Ze Chang [b], Shan He [b], Erik Schlangen [b], Iulia C. Mihai [a], Anthony Jefferson [a]

[a] School of Engineering, Cardiff University, Cardiff CF24 3AA, UK
[b] Faculty of Civil Engineering and Geosciences, TUDelft, Delft 2628 CN, the Netherlands

ARTICLE INFO

Keywords:
Lattice simulations
Self-healing
Fracture process
Numerical analysis

ABSTRACT

This paper describes the development of a discrete lattice model for simulating structures formed from self-healing cementitious materials. In particular, a new approach is presented for simulating time dependent mechanical healing in lattice elements. The proposed formulation is designed to simulate the transient damage and healing behaviour of structures under a range of loading conditions. In addition, multiple and overlapping damage and healing events are considered. An illustrative example demonstrates the effects of varying the healing agent curing parameters on the computed mechanical response. The model is successfully validated using published experimental data from two series of tests on structural elements with an embedded autonomic self-healing system. The *meso*-scale model gives detailed information on the size and disposition of cracking and healing zones throughout an analysis time history. The model also provides an accurate means of determining the volume of healing agent required to achieve healing for all locations within a structural element. The importance of the information provided by the model for the design of self-healing cementitious material elements is highlighted.

1. Introduction

Recent developments in biomimetic cementitious materials, and the potential benefits they offer, have been reported in a number of articles [1–4]. Alongside this experimental and material development work, a certain amount of research has been undertaken on numerical models for simulating the behaviour of self-healing materials [5–7]. These models are useful for understanding the behaviour and optimizing the design parameters of these materials, and also will be needed for designing biomimetic structures. A number of models have been developed for simulating the behaviour of self-healing systems using continuum damage healing mechanics (CDHM) [8–12]. An advantage of CDHM models is that damage and healing are considered directly with variables (scalars or tensors) that represent the corresponding physical processes. In some models, the evolution of healing is considered with healing surfaces that are counterparts to damage surfaces [10,12], whilst in others, healing is taken directly as a proportion of the damage variable(s) [8]. An alternative approach, explored by Davies and Jefferson [13], used micromechanics to simulate directionally-dependent microcracking and healing in cementitious materials. Their model was based on the assumption that healing agent fully

* Corresponding author.
E-mail address: Sayadimoghadams@cardiff.ac.uk (S. Sayadi).

https://doi.org/10.1016/j.engfracmech.2023.109632
Received 17 April 2023; Received in revised form 7 August 2023; Accepted 11 September 2023
Available online 20 September 2023

cures in microcracks at a given time after the cracks form. The aforementioned models consider healing to be instantaneous and do not allow for simultaneous damage and healing.

A number of investigators have explored healing in discrete cracks in quasi-brittle materials using cohesive crack models. Some of these models assume healing to be instantaneous [14] whilst others assume it to be a rate-dependent process [15]. Ponnusami et al. [14] developed a model that is able to simulate multiple healing events using the cohesive zone approach and presented a set of examples that considered cracking and healing behaviour in specimens subject to different loading conditions.

Most models developed to date are not able to simulate rate-dependent healing alongside simultaneous damage and healing processes. An exception to this is the coupled finite model developed by the numerical modelling research team at Cardiff University [16] who used an element with an embedded strong discontinuity and a cohesive zone constitutive formulation to represent the simultaneous time dependent cracking and healing responses of a number of concrete test specimens with embedded vascular networks.

The models discussed above consider cracking and healing using continuum mechanics or simulate macrocracks with the cohesive zone approach. The focus of the present work is on simulating self-healing cementitious materials at micro- and *meso*-scales. The micro- and meso- structures of these cementitious composites are governed by the material composition, which comprises discrete aggregate particles, cementitious matrix and pores [17–19]. Before discussing different approaches for representing these materials explicitly at sub-macro scales, the chemical and physical processes associated with cracking -synonymous with damage- and healing behaviour should be mentioned. These processes include i) crack initiation and propagation, ii) healing activation, iii) healing-agent transport within the crack and surrounding cementitious matrix, and finally iv) curing and solidification of healing materials.

One of the first and most effective methods used for modelling cementitious materials at micro- and meso- scales is the Lattice approach, pioneered by Schlangen and Van Mier [20]. Their initial 2D work was extended to 3D and expanded to include heterogeneous systems [21]. This latter 3D version has been named the 'TUDelft Lattice model'. Other investigators have developed lattice-type approaches and there are now three main categories of Lattice model; the Lattice Spring Model (LSM) [22], the Lattice Discrete Particle model (LDPM) [23] and the original Lattice Beam network Model (LBM) [24]. The LBM has been used extensively to investigate fracture and transport processes in cementitious materials [20,25–30]. This work demonstrated that the lattice approach can successfully simulate the fracture behaviour observed in a range of experiments on quasi-brittle materials, including uniaxial tensile and compression, three- and four-point bending, cylinder splitting, and double edge notch tests. Also, by using pipe elements in combination with lattice beam elements, Šavija et al.[25] and Singla et al. [27] successfully simulated chloride ingress processes in cracked concrete specimens.

Qian et al. [31] furthered the scope of LBM models by showing that they could be used as a sub-scale model that governs the effective constitutive behaviour of an upscaled macroscopic analysis. They generated cement paste microstructures using the HYMOSTRUCT3D model. The geometry and positions of aggregate particles were obtained by using the ANM computer model [32]. The mechanical properties of each phase were derived using nano indentation tests. More recent work has shown that the lattice framework can successfully describe the multiphase microstructure of cement paste [33]. In this work, the authors assigned material properties according to the level of hydration of each cement-paste phase and compared experimentally observed fracture processes with model results. These aforementioned studies proved the efficacy of the lattice approach for simulating damage processes at multiple scales in cementitious materials.

Lv et al. [34] investigated the triggering mechanism of encapsulated self-healing systems using the LBM approach. They characterised shell-interlayer cementitious properties by nanoindentation mapping and assigned the properties thereby derived to corresponding lattice elements. They showed that the numerical results were in good agreement with the experiment data. In another study, the overall mechanical properties of encapsulated cementitious materials, formed using PLA capsules, were investigated by [35].

In a recent study, Cibelli et al. [36] simulated autogenous healing in cementitious materials using the LDPM. The authors considered fracture, moisture transport and hydration processes with a Hygro-Thermo-Chemical formulation. They modelled self-healing in dog bone shaped and double-edged notched prismatic specimens and showed that numerical results were in a good agreement with the experimental data.

The research described in this paper involved deriving an enhanced formulation for simulating time-dependent crack-healing using the lattice approach, which provides detailed information on the nature and extent of damage and healing zones at the *meso*-scale in cementitious structural elements. The resulting model was implemented and validated in the TUDelft lattice program. In the remainder of this paper, the methodology for simulating cracking and healing is explained in section 2. The ability of the model to simulate the behaviour of self-healing systems for a range of damage and healing scenarios is illustrated in section 3. The principal conclusions from the study are presented in section 4.

2. Methodology

The discrete lattice model used for the present work employs multiple beam elements with different properties to represent the micro-structural phases of a cementitious composite. Before describing a new approach for simulating time dependent healing, an overview is provided of the lattice theory along with the method used to simulate fracture.

2.1. Lattice beam network model

The domain is discretised with beam elements which connect a set of randomly positioned nodes. The mesh of beam elements is generated using a Delaunay triangulation algorithm which simultaneously determines the corresponding Voronoi cells [21], as

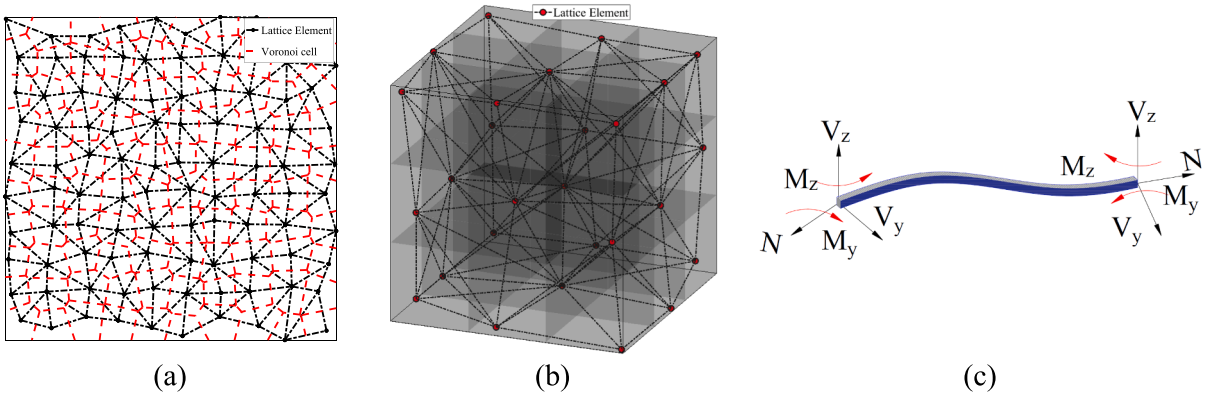

Fig. 1. Illustration of the LBM, a) 2D lattice network with elements and Voronoi cells, b) 3D Lattice structure and c) an element in 3D space.

illustrated in Fig. 1. This procedure involves dividing the domain into cubic sub-cells of specified size. The mesh nodes are then positioned based on the desired level of randomness in each sub-cell. Subsequently, nodes are connected using Delaunay triangulation [37,38].

The mechanical properties of each beam element are determined from experimental tests on concrete specimens (e.g. cylinder compression, cylinder splitting and direct tension tests). For the simulations described in this paper, it is assumed that the material properties throughout the domain are uniform. However, in case of a multiphase system, it would be possible to assign separate properties to the elements corresponding to their material phase (e.g. coarse aggregate, fine aggregate and hardened cement paste). The skeletal finite element system, which is sparse in nature, is assembled in compressed row format [39,40]. Initially, the sequential linear solution procedure was used to solve the nonlinear system of equations, but this was later modified to accommodate the new healing procedure, as explained in Section 2.5. The linearised equation system for each iterative step is solved using a Jacobi pre-conditioned conjugate gradient solver.

The basic method used to simulate damage in the conventional Lattice model is to remove elements from the structural system when the internal representative stress, defined in equation (3), exceeds the damage threshold strength (Section 2.2). This is in contrast to continuum damage mechanics in which a damage variable (ω) varies continuously from zero (no damage) to unity (fully damage) at a material point. In damage mechanics terms, the classical lattice approach would be consistent with the damage variable for an entire element changing instantaneously from zero to one when the element fracture criterion is met. In this study, the conventional lattice approach has been modified to simulate progressive element-level damage in a step-wise (or segmented) fashion for incremental prescribed displacements. This involves the element damage variable being increased in discrete steps from zero to one. Details of this procedure are provided in Section 2.3. In addition, rate dependent damage and healing behaviour has been introduced into the model, as explained in Section 2.4.

2.2. Standard LBM fracture

A standard LBM mesh is illustrated in Fig. 1. The static equilibrium equation for an undamaged linear elastic lattice beam element is as follows:

$$\widehat{\mathbf{K}}_0\widehat{\mathbf{u}} = \widehat{\mathbf{f}} \tag{1}$$

where $\widehat{\mathbf{K}}_0$, $\widehat{\mathbf{u}}$ and $\widehat{\mathbf{f}}$ are the element undamaged stiffness matrix, nodal displacement vector and force vector respectively, noting that ̂denotes element level variables.

The global equation system is obtained by assembling the contributions from each beam element, as follows:

$$\mathbf{K}_{G0}\mathbf{u} = \mathbf{f} \tag{2}$$

where $\mathbf{K}_{G0}$ is the intact global stiffness matrix, and $\mathbf{u}$ and $\mathbf{f}$ are the global displacement and force vectors respectively.

Lattice beam elements are removed when the representative stress (σ), as given by equation (3), exceeds the damage threshold strength of the element (f_t).

$$\sigma = \alpha_N\frac{N}{A} + \beta \times max\left(\frac{|M_i|}{W_i}\right) \tag{3}$$

where N and M are the maximum axial force and bending moment of the beam section respectively, A is the cross-sectional area and W is elastic section modulus; α_N and β govern the normal and flexural stress contributions to the equivalent stress respectively, and are set to $\alpha_N = 1$ and $\beta = 0.05$, based on the values given by Chang et al. [41] for cementitious materials.

Beam elements are removed sequentially such that, at any point in the analysis, the element with the highest representative stress is

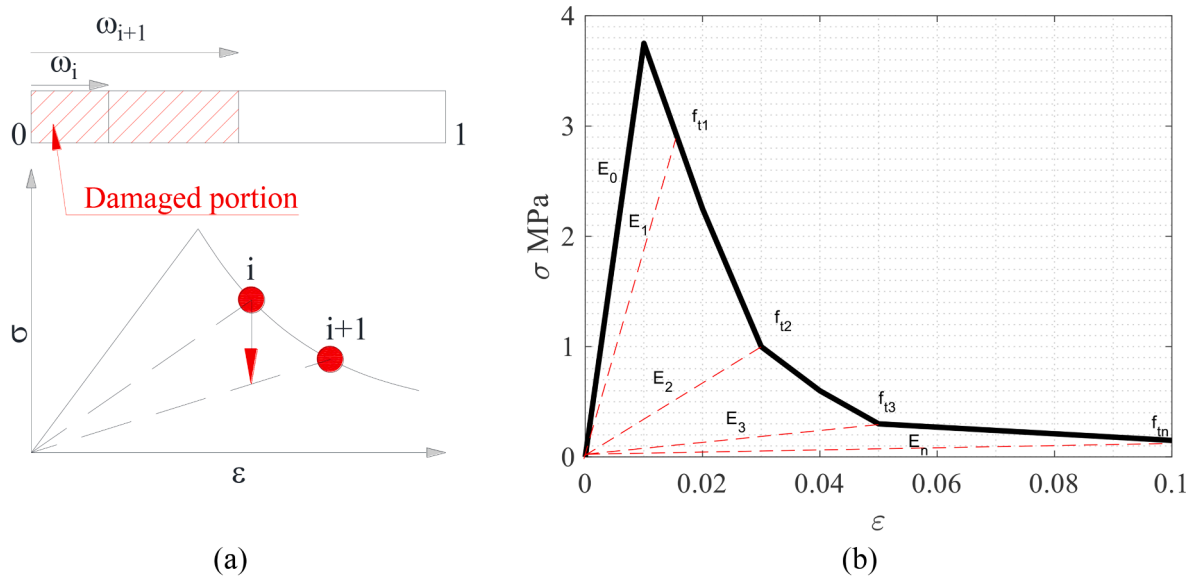

Fig. 2. Stepped softening approach. a) schematic procedure and b) the softening representation of the considered materials in this study.

removed. The solution procedure is sequentially linear with one element being removed per iteration until there are no beams left that exceed the damage threshold.

The assembled equilibrium equation system from equation (2), modified to account for fractured elements, is as follows:

$$\mathbf{K}_{G\omega}\mathbf{u} = \mathbf{f}$$

where $\mathbf{K}_{G\omega}$ is the global stiffness matrix updated for damaged (or fractured) elements.

It is noted that in the standard LBM fracture approach, the stiffness matrix of a fractured beam element is null, i.e. $\widehat{\mathbf{K}}_{\omega} = 0$**.** Further details of how the standard LBM simulates the fracture behaviour of quasi-brittle can be found in [42].

2.3. Progressive damage

The standard LBM was later extended by Schlangen and co-workers [20,43,44] to capture the softening behaviour of concrete using a multi linear constitutive material law, which was assigned to each lattice beam element, such that an element can experience partial -rather than full- damage at a particular time. This method has now been extended to account for the softening behaviour of an element subjected to incremental prescribed displacements in a way that is compatible with incremental-iterative solution procedures.

The damaged element stiffness matrix is obtained from:

$$\widehat{\mathbf{K}}_{\omega} = (1-\omega)\widehat{\mathbf{K}}_0 \tag{5}$$

ω varies in a step-wise manner and is related to the initial and secant elastic moduli (E_0 and E_i respectively), as follows:

$$\omega = 1 - \frac{E_i}{E_0} \tag{6}$$

where i denotes the step number.

The stepped damage procedure determines E_i from the corresponding representative strain (ε_i); noting that $\varepsilon_i = \widetilde{u}_i/L_e$, where $\widetilde{u}_i$ is the representative element relative displacement and L_e the element length. This method employs a stress-representative-strain softening curve based on experimental data appropriate for the materials that have been considered in this paper, as illustrated in Fig. 2b.

In the progressive damage case, the global stiffness matrix ($\mathbf{K}_{G\omega}$) is formed from the assembled element matrices ($\widehat{\mathbf{K}}_{\omega}$), noting that ω is null for undamaged elements.

2.4. Time-dependent healing

Healing is associated with chemical processes that involve (i) healing agent curing in autonomic systems, or (ii) further hydration of unhydrated particles in autogenous self-healing. In both cases, healing is a time dependent phenomenon which involves the diffusion and advection of healed material to and within the cracked area. It has been shown that the progress of healing in many biomimetic

cementitious materials can be represented adequately with an exponential healing function [16,45,46]. This has been used in the present work to enhance the TUDelft-Lattice model to include transient healing. This is accomplished by recovering the properties of damaged elements over time and by allowing for the permanent relative displacements that occur when healing agent cures in an open crack. When damaged elements heal, the system stiffness matrix changes; however, the crucial point is that in a healing sub-step the internal forces should not be changed. This is because mechanical healing alone should not cause a change in the stress or strain energy. The basic assumption is that the healing agent in an open-crack cures in a stress-free condition. This ensures that the model does not violate the second law of thermodynamics [7] and, for a lattice system, this condition implies that the internal forces remain constant during a healing step. The model is based on the assumptions that (i) an adequate amount of healing agent is available to fill the crack fully, and (ii) the transport of healing agents to the crack is instantaneous.

To allow for healing, the basic element equilibrium equation (1) is modified, as follows:

$$\widehat{\mathbf{K}}_{\omega}\widehat{\mathbf{u}} + \widehat{\mathbf{K}}_{\mathrm{h}}(\widehat{\mathbf{u}} - \widehat{\mathbf{u}}_{\mathrm{h}}) = \widehat{\mathbf{f}} \tag{7}$$

where $\widehat{\mathbf{K}}_{\mathrm{h}}$ is the healed element stiffness matrix and $\widehat{\mathbf{u}}_{\mathrm{h}}$ is the element healed displacement vector. $\widehat{\mathbf{u}}_{\mathrm{h}}$ physically represents the width of the cured healing agent zone in a crack (generally equally to the crack width) at the time the crack is healed.

In the absence of re-damage, the element healing matrix at a time t is given by:

$$\widehat{\mathbf{K}}_{\mathrm{h}}(t) = \widehat{\mathbf{K}}_{\mathrm{h}\infty}\left(1 - e^{-\langle t - t_0\rangle/\tau}\right) \tag{8}$$

where τ is a curing time constant, t is the current time, t_0 is the healing initiation time, $\widehat{\mathbf{K}}_{\mathrm{h}\infty}$ is the ultimate healing matrix and $\langle\rangle$ denote Macaulay brackets.

In order to allow for multiple healing cycles and account for the gradual accumulation of the healing displacement vector, equation (8) is introduced into equation (7) and the second term in the latter is re-written as the following summation of convolution integrals, as follows:

$$\widehat{\mathbf{K}}_{\mathrm{h}}(\widehat{\mathbf{u}} - \widehat{\mathbf{u}}_{\mathrm{h}}) = \widehat{\mathbf{f}}_{\boldsymbol{uh}}(t) = \sum_{i=1}^{n}\int_{t_0(i)}^{t}\frac{\widehat{\mathbf{K}}_{\mathrm{h}}e^{-\frac{(s-t_0(i))}{\tau}}}{\tau}(\widehat{\mathbf{u}}(t) - \widehat{\mathbf{u}}_{\mathrm{h}}(s))ds \tag{9}$$

where n represents the number of healing cycles, $\widehat{\mathbf{u}}_{\mathrm{h}}(s)$ is the healed element displacement at the specific time of the curing (s), and the first term of the right hand side is based on the derivative of equation (8), i.e. $\frac{\partial\widehat{\mathbf{K}}_{\mathrm{h}}(t)}{\partial t} = \frac{\widehat{\mathbf{K}}_{\mathrm{h}}e^{-\frac{t}{\tau}}}{\tau}$, which represents the incremental stiffness regain.

The assembled equation system for the damage transient healing case is as follows:

$$\mathbf{K}_{\mathrm{G}\omega}\mathbf{u} + \mathbf{K}_{\mathrm{h}}(\mathbf{u} - \mathbf{u}_{\mathrm{h}}) = \mathbf{f} \tag{10}$$

where $\mathbf{u}_{\mathrm{h}}$ is the global healed displacement vector and $\mathbf{K}_{\mathrm{h}}$ is the assembled healed stiffness matrix. As mentioned earlier, the internal forces in the system should not change during a healing step. This criterion imposes an extra constraint on the global and local equation systems. Theoretically, $\mathbf{u}_{\mathrm{h}}$ could be based on the relative displacement in an element at the time an increment of healing occurs, i.e. based directly on $\mathbf{u}_{\mathrm{h}}$ from the convolution integral in equation (9). However, this would involve storing a large amount of information and undertaking excessive computations involving the summation of all element healing displacement increments for all healing steps up to the step under consideration. An alternative, and far more tractable, solution is to apply the thermodynamic constraint (zero stress change at a healing step) to the global equilibrium equation. In this way there is no need to have a time history record of the element displacement vectors for the whole healing process and only the information from the previous step is required for an update. The internal force vector, allowing for the update in the global nodal healing displacement ($\mathbf{u}_{\mathrm{h}}$), is given by:

$$\mathbf{f}_{\mathrm{uh}} = \mathbf{K}_{\mathrm{h}}(\mathbf{u} - \mathbf{u}_{\mathrm{h}}) \tag{11}$$

Since there should be no change in nodal forces during a healing step, the virtual offset displacement can be derived from equation (11), as follows:

$$\mathbf{u}_{\mathrm{h}} = \mathbf{u} - \mathbf{K}_{\mathrm{h}}{}^{-1}\mathbf{f}_{\mathrm{uh}} \tag{12}$$

2.5. Damage-healing solution algorithm

When solving the system, it proves convenient to group the stiffness terms from equation (7), that pre-multiply $\widehat{\mathbf{u}}$ and $\widehat{\mathbf{u}}_{\mathrm{h}}$, separately and to shift the terms associated with $\widehat{\mathbf{u}}_{\mathrm{h}}$ to the righthand side of the equation, as follows:

$$\widehat{\mathbf{K}}_{\omega\mathrm{h}}\widehat{\mathbf{u}} = \widehat{\mathbf{f}} + \widehat{\mathbf{f}}_{\mathrm{h}} \tag{13}$$

where $\widehat{\mathbf{K}}_{\omega h} = \widehat{\mathbf{K}}_{\omega} + \widehat{\mathbf{K}}_{h}$ and $\widehat{\mathbf{f}}_{\mathrm{h}} = \widehat{\mathbf{K}}_{\mathrm{h}}\widehat{\mathbf{u}}_{\mathrm{h}}$.

The global system counterpart to equation (13) is then:

$$\mathbf{K}_{\omega\mathrm{h}}\mathbf{u} = \mathbf{f} + \mathbf{f}_{\mathrm{h}} \tag{14}$$

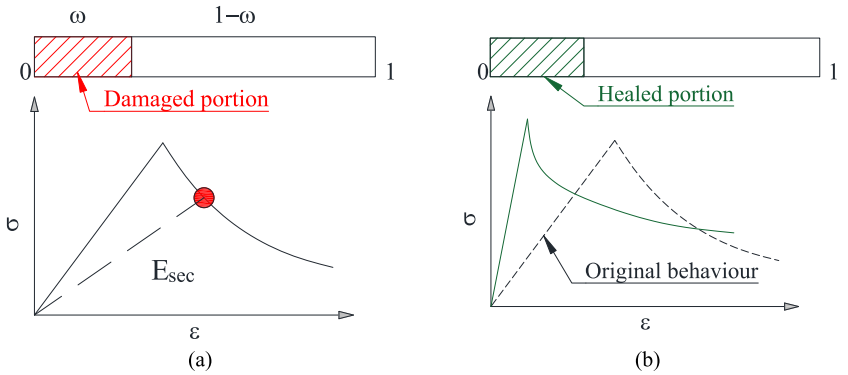

Fig. 3. Schematic illustration of healing for a partial damaged element, a) partially damaged element at time of healing, and b) healed element.

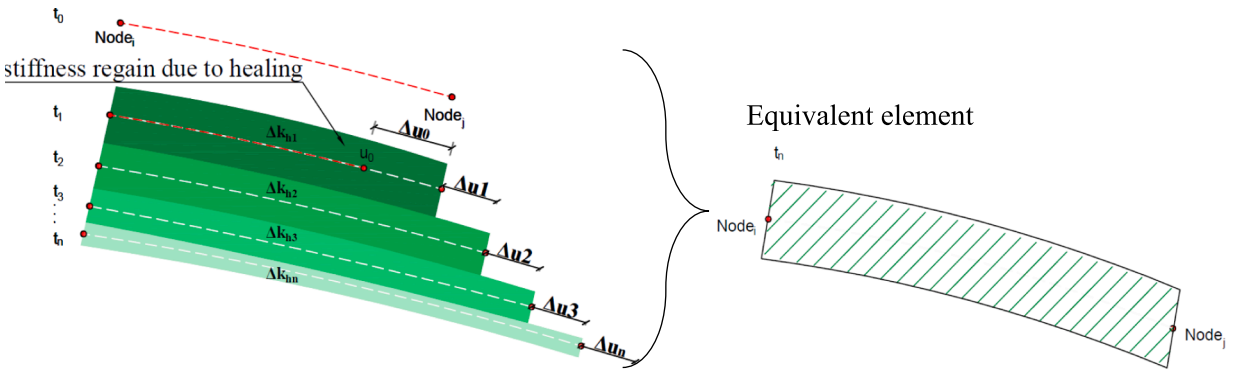

Fig. 4. Sequence stiffness regain due to rate dependent healing procedure.

where $\mathbf{K}_{\omega h} = \mathbf{K}_{\omega} + \mathbf{K}_{h}$ and $\mathbf{f}_{h} = \mathbf{K}_{h}\mathbf{u}_{h}$.

The overall problem is solved using a standard incremental-iterative solution algorithm [47], with each increment of the solution being associated with a time step (p).

The healed stiffness matrix from the summed convolution integrals in equation (9) is evaluated at each time step using the recursive scheme described by Mergheim and Steinmann [48]. The elements available for healing include those that have partially healed but not re-damaged, as well as those newly damaged elements for which healing has been initiated. Allowing for the current and previous damage states, the healed stiffness matrix increments for the first and subsequent healing steps are given by equations (15) and (16) respectively, as follows:

$$\Delta\widehat{\mathbf{K}}_{h_1} = \widehat{\mathbf{K}}_{h\infty}(1 - e^{-\frac{\Delta t}{\tau}})\omega_p, \tag{15}$$

$$\Delta\widehat{\mathbf{K}}_{h_p} = \Delta\widehat{\mathbf{K}}_{h_{p-1}} e^{-\frac{\Delta t}{\tau}} \frac{\omega_p}{\omega_{p-1}}, \tag{16}$$

The healed stiffness matrix increment is added to the current undamaged – healed stiffness matrix, as follows:

$$\widehat{\mathbf{K}}_{\omega h p} = \widehat{\mathbf{K}}_{\omega h p-1} + \Delta\widehat{\mathbf{K}}_{h_p} \tag{17}$$

The healed element force vector is then calculated from the healed stiffness increment at each time step, as follows:

$$\widehat{\mathbf{f}}_{h_p} = \widehat{\mathbf{f}}_{h_{p-1}} + \Delta\widehat{\mathbf{K}}_{h_p}\widehat{\mathbf{u}}_{h_p} \tag{18}$$

When a healed element is re-damaged, the stiffness and healed internal force terms are updated proportionally to the level of re-damage thus, re-healing always commences from a null state. The calculation procedure is illustrated schematically in Fig. 3. This figure shows the equivalent healed element status in terms of the regained stiffness and the internal stress. Since curing is assumed to be an exponential process, the stiffness regain increment is highest for the first step and then gradually reduces in subsequent steps. This is illustrated in Fig. 4, in which the darker the colour the greater the proportion of healing over a time step. At a specific time-step, the overall regained healing stiffness is the summation of the stiffness increments throughout the healing history.

The solution process comprises two sub-steps. The first sub-step, named the 'mechanical step', determines the global displacement vector and damage variable of each element. This requires iterations until the overall damage has reached a steady state. The second

Table 1
Material properties for uniaxial example test.

Properties Example	$E_{m,h}$(MPa)	$f_{tm,h}$(MPa)	$\nu_{m,h}$(MPa)	t_{hi}* (s)	τ(s)			Sample dimensions (mm)
Single healing	29501.6	3.4	0.25	400	1	100	2000	50 × 50 × 50
Re-healing	29501.6	3.4	0.25	200	1	60	1000	50 × 50 × 50

*t_{hi} = Time, after the start of the test, at which healing is initiated.

sub-step is the 'healing step'. In this sub-step, the global displacements are assumed to remain constant whilst the stiffness matrices and $\mathbf{u}_{\mathrm{h}}$ are updated for healing. This procedure is shown schematically in Fig. 4 and is illustrated for a one-dimensional problem in Appendix A.

A preconditioned Conjugate Gradient solver is used to solve the assembled system of equations as well as to determine $\mathbf{u}_{\mathrm{h}}$ at each healing step, the latter being the solution of equation (12).

During a solution, the program stores only the current element damage and healing variables, nodal displacement vector and force vector. The global system stiffness matrix is assembled at each step prior to the solution of the current equation system. This makes the algorithm efficient in terms of memory storage and computational cost.

The following algorithm presents the steps of the numerical implementation of model for a general rate dependence healing scenario which considers the partial damage-healing case.

Algorithm 1 Rate dependent healing algorithm.

	$Inpt: E, G, f_{limit}, E_h, G_h, f_{limit}$. (Element mechanical properties)	Enter, required input parameters
1:	$\boldsymbol{for\ i = 1 : N_{healed\ elements}}$	Loop over damaged elements at each step
2:	$if\ \ element\ state_{eletag(i)} = 0$	First healing time step
3:	$\Delta\widehat{\mathbf{K}}_{\mathrm{h1}} = \widehat{\mathbf{K}}_{\mathrm{h}\infty}\left(1 - e^{-\frac{t}{\tau}}\right)\omega$	Stiffness increment at the first healing time step for a partially damaged element
6:	$\widehat{\mathbf{f}_{\mathrm{h}}} = 0$	Initialize internal healing force
7:	$element\ state_{eletag(i)} = initial\ state$	Update element state
8:	$\boldsymbol{else}$	Further healing due to curing
9:	$\Delta\widehat{\mathbf{K}}_{\mathrm{h_p}} = \Delta\widehat{\mathbf{K}}_{\mathrm{h_{p-1}}} e^{-\frac{\Delta t}{\tau}} \frac{\omega_p}{\omega_{p-1}}$	Updating the healing stiffness increment due to curing and partially re-damaging
13:	$\boldsymbol{end}$	
14:	$\boldsymbol{end}$	
15:	$\widehat{\mathbf{K}}_{\omega h_p} = \widehat{\boldsymbol{K}}_{\omega h_{p-1}} + \Delta\widehat{\boldsymbol{K}}_{h_p}$	Update local stiffness matrix
15:	$\mathbf{K}_{\omega\mathrm{h}} = \mathbf{K}_{\omega\mathrm{h}} + \Delta\mathbf{K}_{\mathrm{h}}$	Update global stiffness matrix
17:	$\hat{\mathbf{f}}_{\mathrm{h}_P} = \hat{\mathbf{f}}_{\mathrm{h}_{p-1}} + \Delta\widehat{\mathbf{K}}_{\mathrm{h}_P}\hat{\mathbf{u}}_{\mathrm{h}_p}$	Calculate accumulated healing force for a healed element
18:	$\mathbf{u}_{\mathrm{h}} = \mathbf{u} - \mathbf{K}_{\mathrm{h}}^{-1}\mathbf{f}_{\mathrm{uh}}$	Update offset displacement vector to satisfy thermodynamics
19:	Set $\mathbf{f} + \mathbf{f_h} = \mathbf{K}_{\omega\mathrm{h}}\mathbf{u}$	Modifying the RHS for the mechanical step
20:	Solve $\mathbf{K}_{\omega\mathrm{h}}\mathbf{u} = \mathbf{f} + \mathbf{f}_{\mathrm{h}}$	Solve linear system of equation
21:	$\hat{\mathbf{f}} = \widehat{\mathbf{K}}_{\omega h_p}\hat{\mathbf{u}} - \hat{\mathbf{f}}_{\mathrm{h}_P}$	Calculate the internal force of healed element
22:	$\boldsymbol{If}\ \hat{\mathbf{f}} > f_t$	Check if any element is broken
23:	$\boldsymbol{for}\ i = 1\ to\ n_{damage}$	Loop over damaged elements at each step
24:	$\widehat{\boldsymbol{K}}_{\omega} = (1 - \omega)\widehat{\mathbf{K}}$	Update local stiffness matrix based on the level of the damage
28:	$\boldsymbol{end}$	

3. Illustrative damage healing responses for different uniaxial strain paths

To illustrate the performance of the enhanced lattice model, the behaviour of a 50 mm self-healing cementitious cube under tensile loading is considered for two different healing scenarios with three healing agents, each with different curing time properties. The first scenario is that healing agent is supplied to the system once at $t = 400$ s and there is a single healing cycle. In the second case, the healing agent is supplied continuously, after its release at 200 s, and multiple healing cycles occur. The properties of the cementitious matrix and the healing agent are given in Table 1. The input parameters required for these simulations are the elastic mechanical properties of cementitious mortar, i.e. Young's modulus (E), Poisson's ratio (ν) and tensile strength (f_t). The parameters used in this simulation, given in Table 1, were taken from the experimental measurements of Selvarajoo et al. [49]. In this numerical example, an incremental displacement is applied to the top of the cube at a rate of 0.001 mm/s. The boundary conditions maintain an average uniaxial state of stress across the specimen.

The mesh used to represent the sample is shown in first image of Fig. 5c. Fig. 5a and 5b show the computed average stress (σ_{av}) and nominal strain (ε_{nom}) responses for three healing-agent cases. The average stress is computed from the total vertical reactions on the top

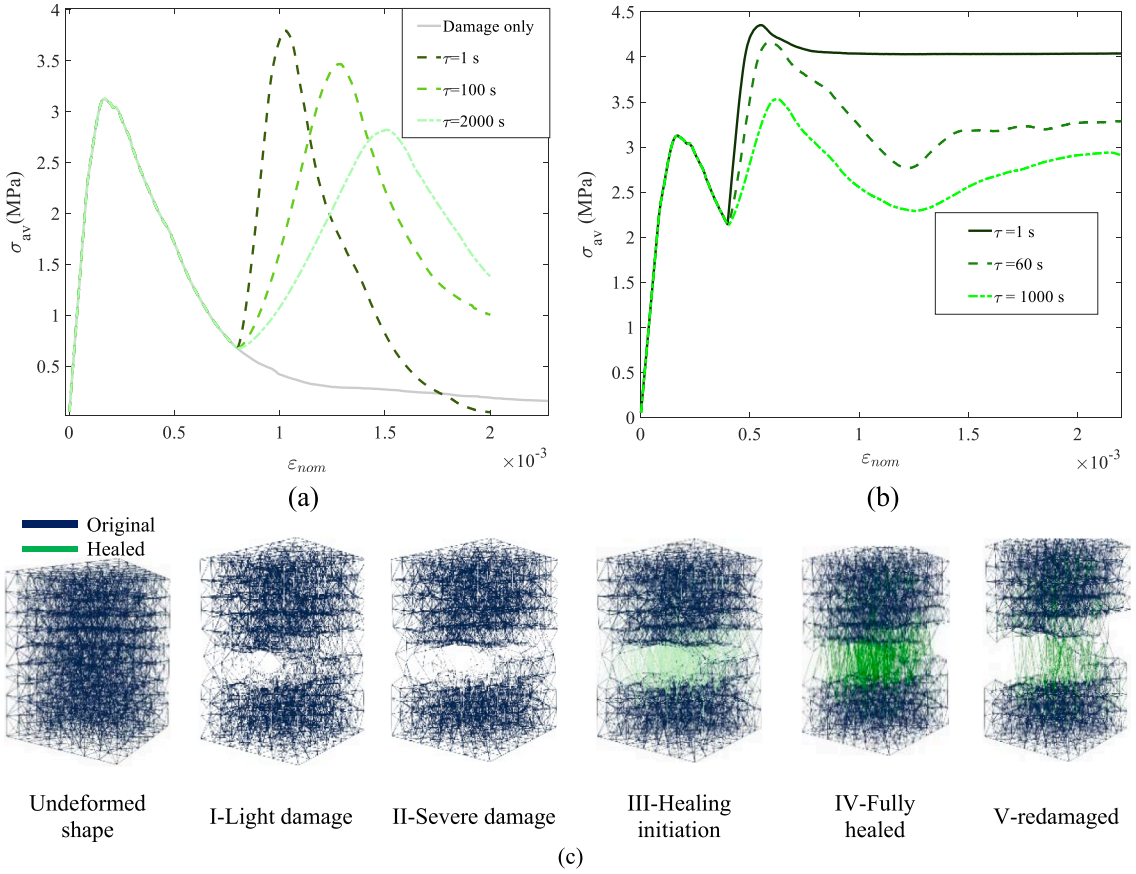

Fig. 5. Constitutive behaviour of self-healing materials derived with the enhanced Lattice model, a) σ_{av}-ε_{nom} curves for single healing scenario, b) σ_{av}-ε_{nom} curves for re-healing re-damaging scenarios and c) Lattice mesh at different phases for healing agent with $\tau = 100s$.

face divided by the cross-sectional area and the strain measure is calculated by dividing the applied displacement by the specimen height. Fig. 5c shows the state of the elements at different stages of the analysis. This figure shows, as expected for a constant loading rate, that the stiffness recoveries and peak post-healed strengths reduce with the rate of healing.

3.1. Computational solution parameters

The starting value of the load step increment was set to 0.0001 mm/sec/sample length. The relative convergence tolerance used was 10^{-6}. The maximum number of iterations was set as 5000. For each iterative step, the previous response was always taken as the initial estimate for the CG solver. The longest element length in all the meshes was 2.5 mm. This ensures that the *meso*-scale meshes are sufficiently fine to capture the cracking process within the fracture process zone for concrete specimens for which the coarse aggregate size was 10 mm.

4. Examples

In order to assess the validity of the proposed approach for simulating the mechanical self-healing behaviour of structural elements formed from self-healing cementitious materials, the model is used to consider two series of experiments undertaken by Selvarajoo et al. [50].These tests comprised a set of notched cube specimens subject to tensile loading (DT series) and a series of notched beams subjected to 3-point loading with (i) a fixed crack width during the healing period (SF series) and (ii) continuous healing with varying crack opening displacement (SO series). The specimens were formed with an autonomic self-healing system that supplied healing agent to damaged zones from an external source.

The material properties used in the analyses are given in Table 2, along with the damage threshold used for the release of the healing agent in each case. The experimental arrangements are shown in Fig. 6 and Fig. 10 for the notched cube and beam specimens respectively.

Table 2
Experiment details and their material properties used for modelling.

Experiment name	$E_{m,h}$(GPa)	f_{tm}(MPa)	f_{th}(MPa)	$\nu_{m,h}$	CMOD at releasing point (mm)	Healing time (s)	τ(s)	Test type
DT-300	30	3.5	3.4	0.2	0.1	300	60	Direct Tension
DT-600	30	3.5	3.4	0.2	0.1	600	60	Direct Tension
SF-120	30	3.0	3.4	0.2	0.15	120	60	3-point bending
SO-0.0005	30	3.0	3.4	0.2	0.075	continuously	60	3-point bending
SO-0.002	30	2.5	3.4	0.2	0.075	continuously	60	3-point bending

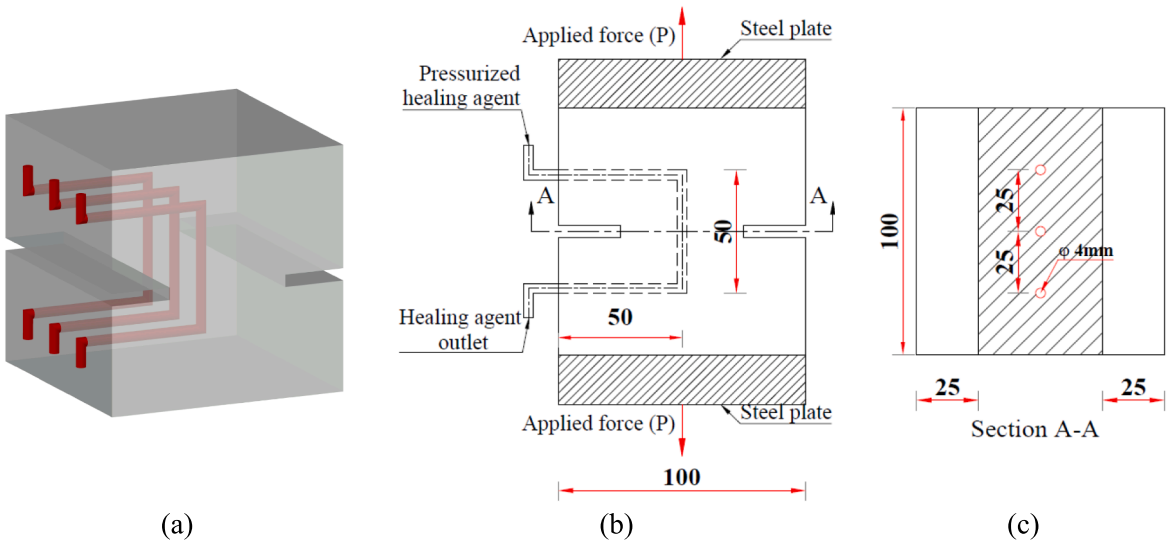

Fig. 6. Experimental arrangement for notched cube tests [49], a) 3D schematic representation, b) front view and c) section view.

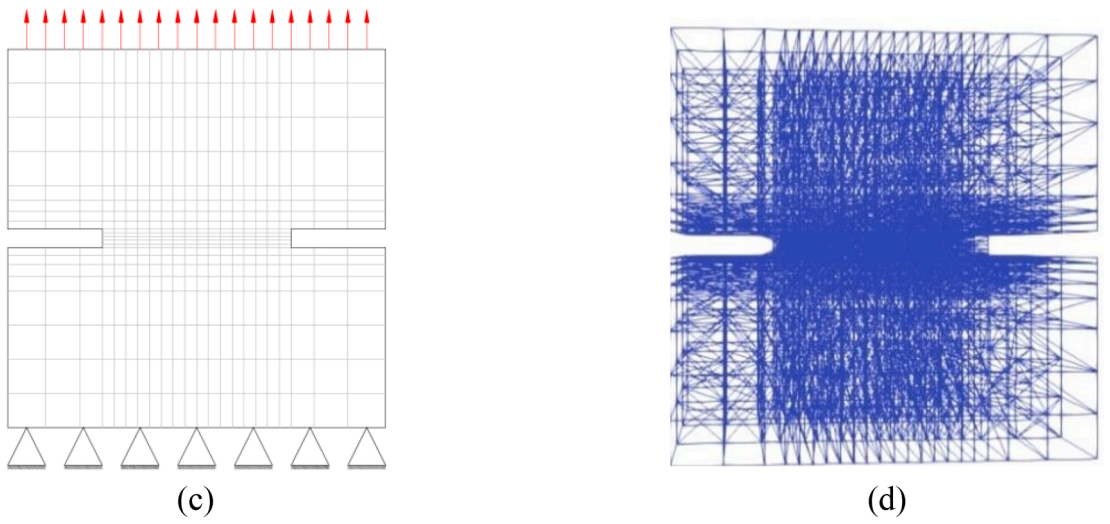

Fig. 7. Boundary condition and mesh configuration, a) mesh and boundary conditions and b) perspective 3D view of the mesh.

4.1. Direct tensile test

A set of doubly notched 100 mm cuboid samples were considered under uniaxial loading. Each sample was loaded in tension until the crack mouth opening displacement (CMOD) reached a limit of 0.1 mm. At this point, the loading was paused and the valve of the pressurized healing agent (cyanoacrylate) supply system was opened. This released the healing agent through the channels embedded in the samples. The healing agent supply was maintained for healing periods of 300 s or 600 s, after which the healing agent supply

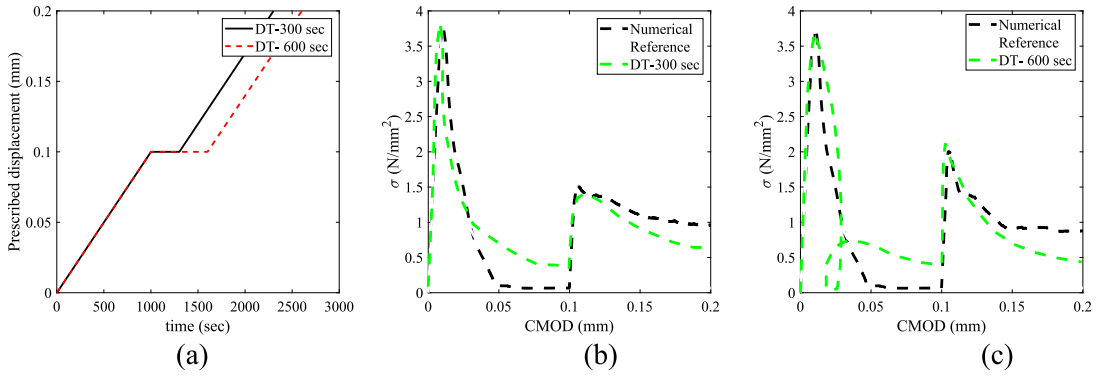

Fig. 8. Numerical simulation results for stress-CMOD of the DT series tests, a) loading protocol, b) stress-CMOD for DT-300 test and c) Stress-CMOD for DT-600 test.

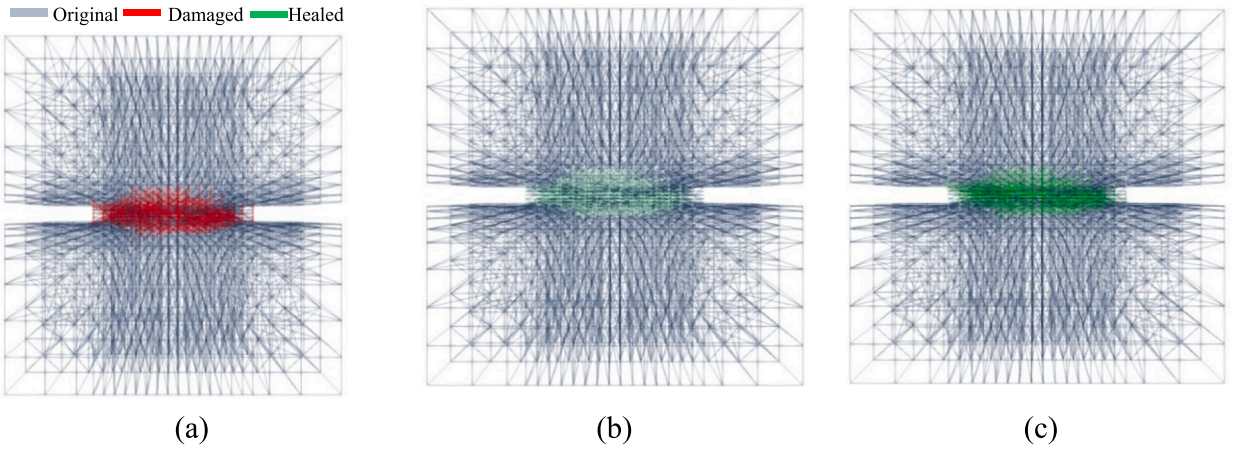

Fig. 9. Damage and healing patterns for DT-600 test, a) damaged state at CMOD = 0.1 mm, b) curing phase at CMOD = 0.1 mm. and c) fully healed phase at CMOD = 0.1 mm.

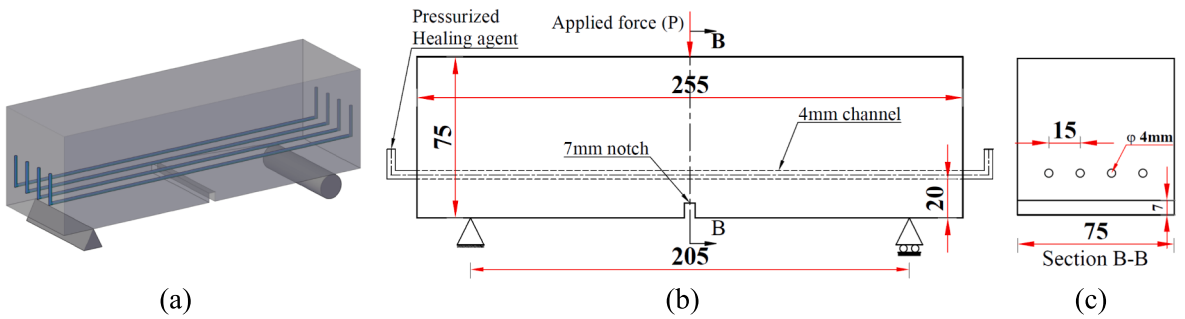

Fig. 10. Experimental setup for notched beam tests, a) 3D schematic view, b) front view and c) beam section.

ceased, and the loading resumed so as to maintain a constant CMOD rate of 0.0001 mm/s. The healing agent properties were taken from [45,49,50].

The mesh and boundary conditions used for the analysis are shown in Fig. 7. The mechanical properties used for the cement matrix and healed material elements are given in Table 2.

The results for two different healing periods are presented in Fig. 8. Based on experimental evidence [49], it is assumed that the healing agent fully cures in a 0.1 mm crack in 600 s but that the curing process is incomplete after 300 s. The results are reported in the form of averaged stress vs CMOD. The average stress is calculated by dividing the normal force by the unnotched area. Plots that show damaged and healed elements before healing initiates (at CMOD = 0.1) and during the healing period are shown in Fig. 8.

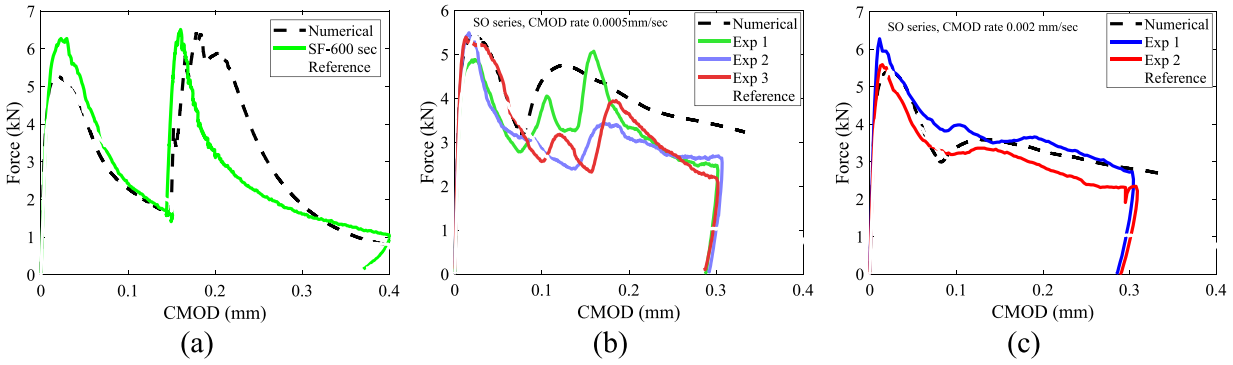

Fig. 11. Notched beam test simulation results, a) SF-120 test results, b) SO series with loading rate 0.0005 mm/s and c) SO series with loading rate 0.002 mm/s.

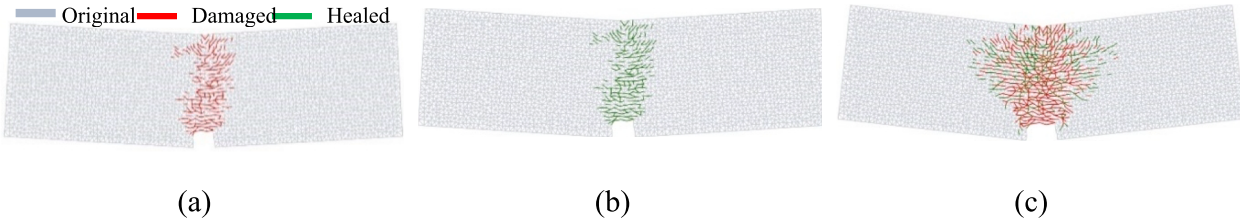

Fig. 12. Crack pattern and system phase in deformed state, a) damaged state CMOD 0.075 mm, b) healed phase CMOD 0.12 mm and c) re-damage-re-healed CMOD 0.2 mm. (all deformations are magnified for clarity).

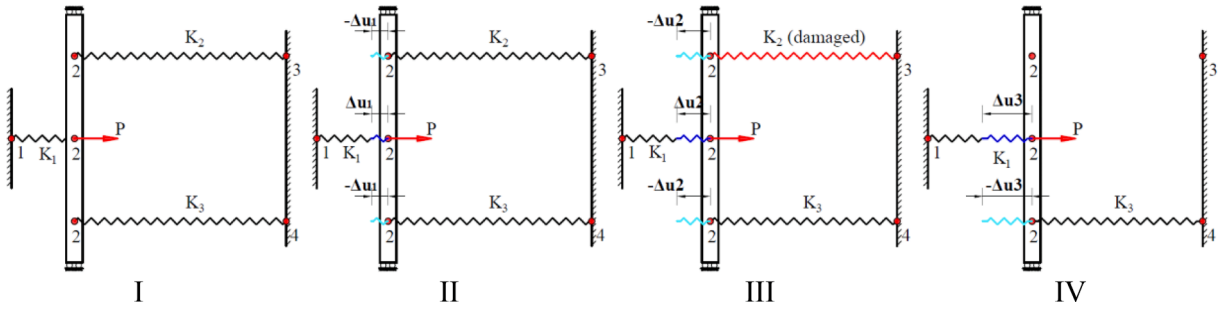

Fig. A1. Schematic procedure for fracture process in lattice.

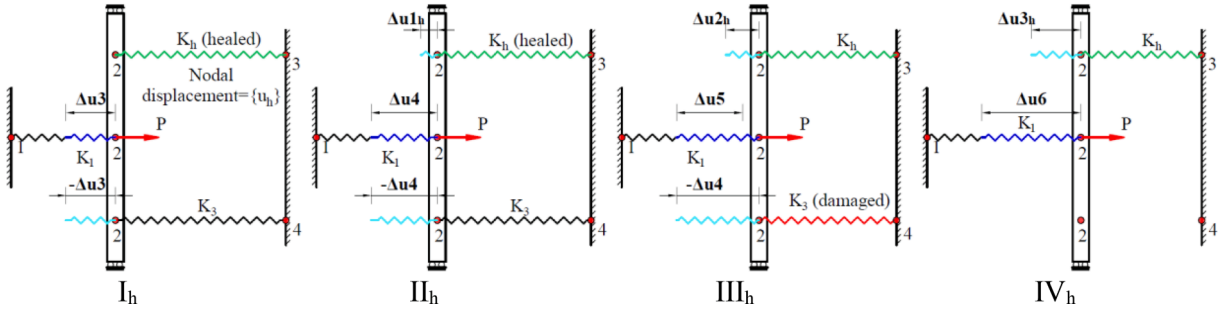

Fig. A2. Schematic procedure for healing implementation in the Lattice.

The results presented in Fig. 8 show that stiffness and strength recoveries are in a good agreement with the experiments. The results (Fig. 8b and 8c) confirm that the model is able to simulate partial healing and the response of specimens subject to different healing periods. It is noted that the numerical simulations allowed for the experimental observation that healing agent was transported to 60%

of the crack area. The plots in Fig. 9 show that the damage-healing zone extends above and below the notch with an overall characteristic dimension of approximately 15 mm.

The information provided by analysing the fracture zone, is used to estimate the amount of required healing agent. For the SF case, based on the element healed displacement ($\widehat{\mathbf{u}}_{\mathbf{h}}$) and cross section area. The required amount of healing agent for this case is 1045 mm^3.

4.2. 3-Point bending test

The notched self-healing beam explored for the second example is illustrated in Fig. 10. Two different healing scenarios were considered, one in which the crack opening displacement remained constant during the healing period (SF tests) and the other for which the CMOD was increased at a constant rate with healing agent supplied at a pressure of 0.5 bar (SO tests). For the former (SF) series, an analysis was undertaken until the CMOD reached 0.15 mm. Healing agent was supplied for a period of 120 s while the CMOD was kept constant, after which, the loading was resumed at a CMOD rate of 0.001 mm/s. For the latter (SO) series, post-crack CMOD rates of 0.0005 and 0.002 mm/s were used, with the analyses being continued until the CMOD reached 0.3 mm. The reason for choosing these two different healing scenarios is to assess the ability of the proposed model to simulate healing for both fixed crack and moving crack scenarios, with the latter involving multiple and simultaneous damage and healing events. The material properties and test parameters are summarised in Table 2.

The results from the fixed crack (SF) analysis are compared with experimental data in Fig. 11a. The numerical response in terms of stiffness and strength recovery is generally in good agreement with the experimental data, although the initial peak in the numerical simulation is slightly greater than the experimental average. The difference is considered to be within the natural variability level for this type of material. The results from the SO series analyses for the two different CMOD rates are compared to the experiment data from three tests with the same parameters in Fig. 11b and 11c. This scenario is much more complex than the fixed crack case since healing and damage events overlap in time. The numerical responses are again in good general agreement with the experimental data and show the ability of the model to capture multiple re-damaging-re-healing events. This can be seen clearly at the end of the graph (Fig. 11b and 11c) where the numerical response tends to an asymptote, although the numerical plots do not exhibit the multiple peaks seen in the experimental data. Plots showing the extent of damage, healing, re-damage and re-healing are presented in Fig. 12a to 12c. It may be seen from these plots that the fracture zone is relatively wide, with a characteristic dimension of approximately 20 mm after the first cracking stage and 60 mm at the final stage after re-healing and re-damage have occurred. It may also be seen also that healing extends to the far reaches of the fracture process zone.

Following the same approach for calculating of the required healing agent volume gives 234 mm^3.

The examples presented in this paper relate to an autonomic healing material; however, the proposed model framework is equally applicable to the simulation of autogenous healing processes. To apply the model to an autonomic problem the healing rate function would need to be determined from the hydration rate of unhydrated cement particles and the rate of formation of other cementitious healing compounds (e.g. portlandite) [44].

The model provides detailed information on the distribution and size of damage and healing zones at the *meso*-scale, along with the associated volume of healing agent required at a particular time in the life of a structural element. These output data are far more refined that those provided by a comparable continuum model. This is essential information for the efficient design of a self-healing system and is also useful for researchers developing new self-healing systems.

The present paper has concentrated on simulating time-dependent mechanical healing at the *meso*-scale but the model could be readily coupled to a transport model to simulate the movement of healing agent through the body of a structural element and within cracks [16].

5. Conclusions

A model has been presented for simulating the response of structural elements formed from self-healing cementitious materials based on the TUDelft lattice framework. The existing LBM has been extended to account for simultaneous and rate-dependent damage and healing processes. The main conclusions from the present study are given below.

- The model is able to replicate the mechanical response of self-healing cementitious materials with good accuracy, including fracture and rate-dependent healing behaviour.
- It is able to simulate multiple healing cycles, as well as overlapping damage and healing processes.
- The *meso*-scale lattice simulations provide valuable information on the size, geometry and disposition of the fracture and healing zones for the full history of a simulation.
- The method provides a viable means of computing the amount of agent required to produce healing at any time within an analysis.
- The mechanical and chemical properties of healing agents have a significant influence on the degree of healing and on the overall response of a self-healing material.
- The rate of applied loading and the healing rate of an agent both influence strongly the mechanical response of a self-healing structural element.
- The experimental and numerical results indicate that, for multiple re-healing-re-damaging scenarios, the overall response reaches an asymptote in which healing and damage increments balance each other.

- The detailed *meso*-scale data provided by the new lattice model would be of considerable value to researchers developing new self-healing material systems, as well as to engineers designing structural elements formed from self-healing materials.

CRediT authorship contribution statement

Sina Sayadi: Writing – original draft, Software, Validation, Visualization, Methodology, Writing – review & editing. **Ze Chang:** Methodology, Writing – review & editing. **Shan He:** Methodology. **Erik Schlangen:** Supervision, Methodology, Conceptualization. **Iulia C. Mihai:** Supervision, Methodology, Conceptualization, Writing – review & editing. **Anthony Jefferson:** Validation, Supervision, Methodology, Conceptualization, Writing – review & editing.

Declaration of Competing Interest

The authors declare that they have no known competing financial interests or personal relationships that could have appeared to influence the work reported in this paper.

Data availability

Data will be made available on request.

Acknowledgment

 This project has received funding from the European Union's Horizon 2020 research and innovation programme under the Marie Skłodowska-Curie grant agreement No 860006.

Appendix A. The 1D illustration

Under further loading, if a healed element is damaged then the global and local healing stiffness matrix, as well as the healing force in the governing equations needed to be updated for considering re-damaging possibility. For a better demonstration, a simplified 1-D case is provided as an example for showing the whole formulation and implementation procedure. Fig. A1 shows the 4 node 1-D structure subjected to a tensile force, at a certain displacement it is assumed that element number 2 would be broken and have this potential to be healed.

In this example the system initial stiffness and equilibrium equations can be written in the form of the following matrix form.

$$\begin{bmatrix} k_1 & -k_1 & 0 & 0 \\ -k_1 & k_1+k_2+k_3 & -k_2 & -k_3 \\ 0 & -k_2 & k_2 & 0 \\ 0 & -k_3 & 0 & k_3 \end{bmatrix} \begin{Bmatrix} u_1 \\ u_2 \\ u_3 \\ u_4 \end{Bmatrix} = \begin{Bmatrix} R_1 \\ P \\ R_3 \\ R_4 \end{Bmatrix} \tag{A1}$$

where k is the lattice beam element stiffness matrix, u is nodal displacement, R is reaction force and P is external force.

At stage III where the second element is assumed to be broken, the system global stiffness matrix is updated as follow.

$$\mathbf{K}_{G\omega} = \begin{bmatrix} k_1 & -k_1 & 0 & 0 \\ -k_1 & k_1+0+k_3 & 0 & -k_3 \\ 0 & 0 & 0 & 0 \\ 0 & -k_3 & 0 & k_3 \end{bmatrix} \tag{A2}$$

At a specific stage (Like Fig. A2) in which the nodal displacements are $\mathbf{u_h}$, it is assumed that the healing would be started. The equilibrium equations for such a system at the healing point are reformulated as noted in equation A(3). Because the healed element is generated in a deformed state, the internal force of healed element is calculated by $k_h(u_2 - u_{2h}) = f_2$.

$$\begin{cases} R_1 = K_1u_1 - k_1u_2 \\ P = -k_1u_1 + k_1u_2 + k_h(u_2 - u_{2h}) - k_h(u_3 - u_{3h}) + k_3u_2 - k_3u_4 \\ R_3 = -k_2(u_2 - u_{2h}) + k_h(u_3 - u_{3h}) \\ R_4 = -k_3u_2 + k_3u_4 \end{cases} \tag{A3}$$

In which k_h is the healed element stiffness matrix. The matrix form of the above series of equations are rewritable in the following format.

$$\begin{bmatrix} k_1 & -k_1 & 0 & 0 \\ -k_1 & k_1+k_h+k_3 & -k_h & -k_3 \\ 0 & -k_h & k_h & 0 \\ 0 & -k_3 & 0 & k_3 \end{bmatrix} \begin{Bmatrix} u_1 \\ u_2 \\ u_3 \\ u_4 \end{Bmatrix} - \begin{bmatrix} 0 & 0 & 0 & 0 \\ 0 & +k_h & -k_h & 0 \\ 0 & -k_h & k_h & 0 \\ 0 & 0 & 0 & 0 \end{bmatrix} \begin{Bmatrix} u_{1h} \\ u_{2h} \\ u_{3h} \\ u_{4h} \end{Bmatrix} = \begin{Bmatrix} R_1 \\ P \\ R_3 \\ R_4 \end{Bmatrix} \tag{A4}$$

In which the adjustment healing force (f_h) is defined as follow.

$$f_h = \begin{bmatrix} 0 & 0 & 0 & 0 \\ 0 & +k_h & -k_h & 0 \\ 0 & -k_h & k_h & 0 \\ 0 & 0 & 0 & 0 \end{bmatrix} \begin{Bmatrix} u_{1h} \\ u_{2h} \\ u_{3h} \\ u_{4h} \end{Bmatrix} \tag{A5}$$

References

[1] Van Tittelboom K, De Belie N. Self-healing in cementitious materials-a review. Materials 2013;6(6):2182–217.
[2] Shields Y, De Belie N, Jefferson A, Van Tittelboom K. A review of vascular networks for self-healing applications. Smart Mater Struct 2021;30(6):063001.
[3] Ferrara L, Van Mullem T, Alonso MC, Antonaci P, Borg RP, Cuenca E, et al. Experimental characterization of the self-healing capacity of cement based materials and its effects on the material performance: A state of the art report by COST Action SARCOS WG2. Constr Build Mater 2018;167:115–42.
[4] De Belie N, Gruyaert E, Al-Tabbaa A, Antonaci P, Baera C, Bajare D, et al. A Review of Self-Healing Concrete for Damage Management of Structures. Adv Mater Interfaces 2018;5(17). https://doi.org/10.1002/admi.201800074.
[5] Pan Z, Ma R, Wang D, Chen A. A review of lattice type model in fracture mechanics: theory, applications, and perspectives. Engng Fract Mech 2018;190:382–409.
[6] Freeman BL, Jefferson AD. Numerical Simulation of Self-Healing Cementitious Materials BT - Self-Healing Construction Materials: Fundamentals, Monitoring and Large Scale Applications. In: Kanellopoulos A, Norambuena-Contreras J, editors., Cham: Springer International Publishing; 2022, p. 151–85. Doi: 10.1007/978-3-030-86880-2_6.
[7] Jefferson T, Javierre E, Freeman B, Zaoui A, Koenders E, Ferrara L. Research Progress on Numerical Models for Self-Healing Cementitious Materials. Adv Mater Interfaces 2018;5:1701378. https://doi.org/10.1002/admi.201701378.
[8] Schimmel EC, Remmers JJC. Development of a constitutive model for self-healing materials. 2006.
[9] Darabi MK, Abu Al-Rub RK, Little DN. A continuum damage mechanics framework for modeling micro-damage healing. Int J Solids Struct 2012;49(3-4):492–513.
[10] Barbero EJ, Greco F, Lonetti P. Continuum Damage-Healing Mechanics with application to self-healing composites. Int J Damage Mech 2005;14:51–81. https://doi.org/10.1177/1056789505045928.
[11] Pan Y, Tian F, Zhong Z. A continuum damage-healing model of healing agents based self-healing materials. Int J Damage Mech 2018;27(5):754–78.
[12] Voyiadjis GZ, Shojaei A, Li G, Kattan P. Continuum damage-healing mechanics with introduction to new healing variables. Int J Damage Mech 2012;21(3):391–414.
[13] Davies R, Jefferson A. Micromechanical modelling of self-healing cementitious materials. Int J Solids Struct 2017;113–114:180–91. https://doi.org/10.1016/j.ijsolstr.2017.02.008.
[14] Ponnusami SA, Krishnasamy J, Turteltaub S, van der Zwaag S. A cohesive-zone crack healing model for self-healing materials. Int J Solids Struct 2018;134:249–63.
[15] Freeman BL, Bonilla-Villalba P, Mihai IC, Alnaas WF, Jefferson AD. A specialised finite element for simulating self-healing quasi-brittle materials. Adv Model Simul Eng Sci 2020;7:32. https://doi.org/10.1186/s40323-020-00171-4.
[16] Freeman BL, Jefferson T. The simulation of transport processes in cementitious materials with embedded healing systems. Int J Numer Anal Meth Geomech 2020;44:293–326. https://doi.org/10.1002/nag.3017.
[17] Zhang M, Jivkov AP. Microstructure-informed modelling of damage evolution in cement paste. Constr Build Mater 2014;66:731–42.
[18] Zhang M, Ye G, Breugel KV. Microstructure-based modeling of permeability of cementitious materials using multiple-relaxation-time lattice Boltzmann method. Comput Mater Sci 2013;68:142–51.
[19] Gan Y, Romero Rodriguez C, Zhang H, Schlangen E, van Breugel K, Šavija B. Modeling of microstructural effects on the creep of hardened cement paste using an experimentally informed lattice model. Comput Aided Civ Inf Engng 2021;36(5):560–76.
[20] Schlangen E, van Mier JGM. Simple lattice model for numerical simulation of fracture of concrete materials and structures. Mater Struct 1992;25:534–42. https://doi.org/10.1007/BF02472449.
[21] Qian Z, Ye G, Schlangen E, van Breugel K. 3D Lattice Fracture Model: Application to Cement Paste at Microscale. Key Engng Mater 2011;452–453:65–8. https://doi.org/10.4028/www.scientific.net/KEM.452-453.65.
[22] Bolander JE, Saito S. Fracture analyses using spring networks with random geometry. Engng Fract Mech 1998;61:569–91. https://doi.org/10.1016/S0013-7944(98)00069-1.
[23] Cusatis G, Pelessone D, Mencarelli A. Lattice Discrete Particle Model (LDPM) for failure behavior of concrete. I: Theory. Cem Concr Compos 2011;33(9):881–90.
[24] Alessandro F, E. BJ, Nicola N.. Lattice Discrete Particle Modeling of Concrete under Compressive Loading: Multiscale Experimental Approach for Parameter Determination. J Engng Mech 2018;144:4018058. https://doi.org/10.1061/(ASCE)EM.1943-7889.0001480.
[25] Šavija B, Farias J, Polder R, Schlangen E. Lattice model as a tool for modelling transport phenomena in cement based composites; 2012.
[26] Schlangen E, Garboczi EJ. New method for simulating fracture using an elastically uniform random geometry lattice. Int J Engng Sci 1996;34:1131–44. https://doi.org/10.1016/0020-7225(96)00019-5.
[27] Singla A, Šavija B, Sluys LJ, Romero RC. Modelling of capillary water absorption in sound and cracked concrete using a dual-lattice approach: Computational aspects. Constr Build Mater 2022;320:125826. https://doi.org/10.1016/j.conbuildmat.2021.125826.
[28] Zhang H, Šavija B, Schlangen E. Towards understanding stochastic fracture performance of cement paste at micro length scale based on numerical simulation. Constr Build Mater 2018;183:189–201. https://doi.org/10.1016/j.conbuildmat.2018.06.167.
[29] Athanasiadis I, Wheeler SJ, Grassl P. Hydro-mechanical network modelling of particulate composites. Int J Solids Struct 2018:130–1. https://doi.org/10.1016/j.ijsolstr.2017.10.017.
[30] Grassl P, Antonelli A. 3D network modelling of fracture processes in fibre-reinforced geomaterials. Int J Solids Struct 2019:156–7. https://doi.org/10.1016/j.ijsolstr.2018.08.019.
[31] Qian Z, Schlangen E, Ye G, van Breugel K. Modeling Framework for Fracture in Multiscale Cement-Based Material Structures. Materials 2017;10. Doi: 10.3390/ma10060587.
[32] Qian Z, Garboczi EJ, Ye G, Schlangen E. Anm: a geometrical model for the composite structure of mortar and concrete using real-shape particles. Materials and Structures/Materiaux et Constructions 2016;49(1-2):149–58.

[33] Xu Y, Gan Y, Chang Z, Wan Z, Schlangen E, Šavija B. Towards understanding deformation and fracture in cementitious lattice materials: Insights from multiscale experiments and simulations. Constr Build Mater 2022;345:128409. https://doi.org/10.1016/j.conbuildmat.2022.128409.
[34] Lv L-Y, Zhang H, Schlangen E, Yang Z, Xing F. Experimental and numerical study of crack behaviour for capsule-based self-healing cementitious materials. Constr Build Mater 2017;156:219–29.
[35] Rodríguez CR, de Mendonça Filho FF, Mercuri L, Gan Y, Rossi E, Anglani G, et al. Chemo-physico-mechanical properties of the interface zone between bacterial PLA self-healing capsules and cement paste. Cem Concr Res 2020;138:106228.
[36] Cibelli A, Pathirage M, Cusatis G, Ferrara L, Di Luzio G. A discrete numerical model for the effects of crack healing on the behaviour of ordinary plain concrete: Implementation, calibration, and validation. Engng Fract Mech 2022;263:108266. https://doi.org/10.1016/j.engfracmech.2022.108266.
[37] Chang Ze, Zhang H, Liang M, Schlangen E, Šavija B. Numerical simulation of elastic buckling in 3D concrete printing using the lattice model with geometric nonlinearity. Autom Constr 2022;142:104485.
[38] Chang Ze, Liang M, Xu Y, Schlangen E, Šavija B. 3D concrete printing: Lattice modeling of structural failure considering damage and deformed geometry. Cem Concr Compos 2022;133:104719.
[39] Zienkiewicz O, Taylor R, Zhu JZ. The Finite Element Method: its Basis and Fundamentals: Seventh Edition. 2013. https://doi.org/10.1016/C2009-0-24909-9.
[40] Barrett R, Berry M, Chan TF, Demmel J, Donato J, Dongarra J, et al. Templates for the Solution of Linear Systems: Building Blocks for Iterative Methods. 1994. Doi: 10.1137/1.9781611971538.
[41] Chang Z. Lattice model for numerical analysis of fracture process of concrete material under various loading conditions, 2019. https://doi.org/10.21012/fc10.235704.
[42] Chang Ze, Zhang H, Schlangen E, Šavija B. Lattice Fracture Model for Concrete Fracture Revisited: Calibration and Validation. Appl Sci 2020;10(14):4822.
[43] Schlangen E. M&S highlight: Schlangen and van Mier (1992), Simple lattice model for numerical simulation of fracture of concrete materials and structures. Mater Struct 2022;55:95. https://doi.org/10.1617/s11527-022-01932-w.
[44] Qian Z. Multiscale Modelling of Fracture Processes in Cementitious Materials. Delft, The Netherlands: Delft University of Technology; 2012.
[45] Jefferson AD, Freeman BL. A crack-opening-dependent numerical model for self-healing cementitious materials. Int J Solids Struct 2022;244–245:111601. https://doi.org/10.1016/j.ijsolstr.2022.111601.
[46] Freeman BL, Jefferson A. A 3D Coupled Finite-Element Model for Simulating Mechanical Regain in Self-Healing Cementitious Materials. J Engng Mech 2023;149:04023038.
[47] Borst De, René MA, Crisfield JJC, Remmers, and Clemens V. Verhoosel.. Nonlinear finite element analysis of solids and structures. John Wiley & Sons; 2012.
[48] Mergheim J, Steinmann P. Phenomenological modelling of self-healing polymers based on integrated healing agents. Comput Mech 2013;52(3):681–92.
[49] Selvarajoo T, Davies RE, Freeman BL, Jefferson AD. Mechanical response of a vascular self-healing cementitious material system under varying loading conditions. Constr Build Mater 2020;254:119245.
[50] Selvarajoo T, Davies RE, Gardner DR, Freeman BL, Jefferson AD. Characterisation of a vascular self-healing cementitious material system: Flow and curing properties. Constr Build Mater 2020;245:118332.